Seismic Trapped Modes in the Oroville and San Andreas Fault Zones

Yong-Gang Li,* Peter Leary, Keiiti Aki, Peter Malin

Three-component borehole seismic profiling of the recently active Oroville, California, normal fault and microearthquake event recording with a near-fault three-component borehole seismometer on the San Andreas fault at Parkfield, California, have shown numerous instances of pronounced dispersive wave trains following the shear wave arrivals. These wave trains are interpreted as fault zone–trapped seismic modes. Parkfield earthquakes exciting trapped modes have been located as deep as 10 kilometers, as shallow as 4 kilometers, and extend 12 kilometers along the fault on either side of the recording station. Selected Oroville and Parkfield wave forms are modeled as the fundamental and first higher trapped SH modes of a narrow low-velocity layer at the fault. Modeling results suggest that the Oroville fault zone is 18 meters wide at depth and has a shear wave velocity of 1 kilometer per second, whereas at Parkfield, the fault gouge is 100 to 150 meters wide and has a shear wave velocity of 1.1 to 1.8 kilometers per second. These low-velocity layers are probably the rupture planes on which earthquakes occur.

Seismic trapped modes in crustal fault zones illustrate the coherent interference phenomenon of wave propagation in a highly fractured low-velocity layer bounded by higher velocity crustal intact rocks. The observation of fault zone–trapped waves can reveal the properties and geometry of the low-velocity layer thought to lie at the heart of the fault zone. Because of the sensitivity of trapped wave excitation to the source location, it allows precise location of seismic events relative to the fault plane and characterization of microearthquake occurrence and properties as a function of position within or outside the fault zone. By these means, monitoring fault zone–trapped waves is particularly useful in the context of earthquake prediction studies.

Although earthquake faults have a waveguide-like structure [a planar central zone of highly damaged rock giving way to progressively more intact rock (*1, 2*)], fault zone–guided waves appear to have not been recognized in surface seismic recordings. The reason may be the geological complexity of the near surface crust and the presence of seismic energy trapped in low-velocity layers. Weathering of crustal rock produces a surface layer of low-velocity material that also acts to trap seismic energy (*1, 3*). The majority of these near surface problems can be avoided by placing seismometers in boreholes at depths of 200 to 300 m.

Fault zone–trapped waves have been recognized in a borehole seismic profiling experiment conducted at a local active normal fault in crystalline rock near Oroville, California (*2*). Observations of both P and S body waves and fault zone–trapped waves allowed a systematic investigation of the fault zone structure, and from this study we developed a simple method with which to model trapped wave observations. For the Oroville experiment, the seismic receiver was located in a borehole that reached the upper edge of the fault at a depth of 305 m (Fig. 1, top). Source points were laid out from the borehole on a radial line normal to and crossing the fault. Using ray tracing, we inverted the body wave travel times to define the fault zone velocity structure in the plane normal to the fault (*2*). When a source was applied on the surface trace of the fault, receivers close to the fault plane recorded fault zone–guided waves (Fig. 2). The ringing, low-frequency trapped waves (L) following the shear body waves (S) are most evident in SH-component seismograms for a sequence of receiver locations arranged up the borehole away form the fault (Fig. 2, top). This signal pattern is symptomatic of a strong velocity contrast between the fault zone and surrounding rocks. The amplitude of the trapped waves decreases with distance away from the fault plane (Fig. 2, middle). The evanescent character of trapped wave energy outside the low-velocity layer is apparent at receivers away from the fault zone. We computed SH/Love fault zone trapped wave forms (Fig. 2, bottom) using a rapid phase shift algorithm (*4*) and Green's function for Love waves (*5*). The results indicate that trapped modes are more sensitive than body waves to low-velocity structures (*2, 4*). Results from range of forward models suggest of the fault zone structure (Fig. 1) that the velocity can be determined within about ±0.1 km/s.

On the San Andreas fault (SAF) at Parkfield, California, a ten-station borehole digital seismic network of three-component instruments (Fig. 3) is operated by the U.S. Geological Survey and the University of California (*6*). The SAF at Parkfield separates two crustal blocks. To the northeast lies the Franciscan block, which contains fluid-rich metamorphosed sea floor sediments. The southwest crustal block is primarily harder and more durable granite, in which seismic velocities are fast. Seismic tomography shows that seismic velocity varies asymmetricly across the fault and suggests that the variation is abrupt at the southwest (granitic) block and gradual at the northeast (Franciscan) block (*1, 3*). The network monitors the fault in anticipation of a magnitude 6 earthquake thought to recur at Parkfield on an approximately 22-year cycle (7). At borehole depths of 200 to 300 m, where seismic background noise and the region of complex geology near the surface may be avoided, detection of small (magnitudes, $M > -0.5$) earthquakes is possible (*8*). As a result of favorable borehole recording conditions, one station (MM), offset 300 m from the surface trace of the SAF, has recorded low-frequency dispersive wave trains characteristic of seismic energy trapped in the low-velocity layer of the fault zone. Two separate trapped

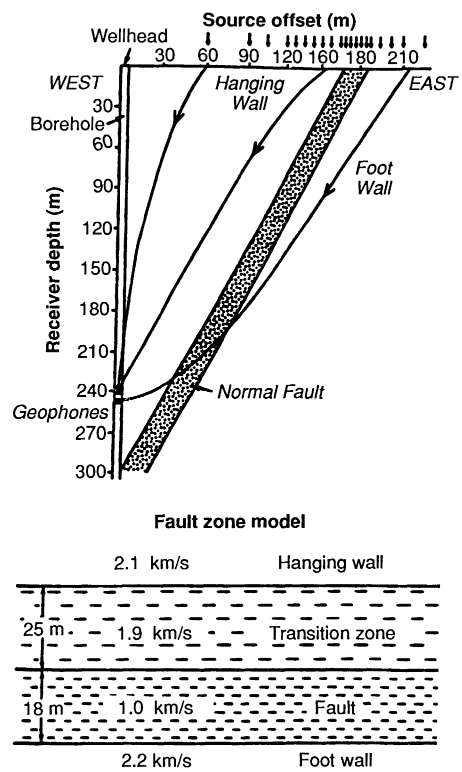

Fig. 1. (**Top**) Fault zone, borehole and source geometry, Oroville, California, borehole seismic profiling experiment. (**Bottom**) Fault zone model parameters (thickness and seismic velocity) for Oroville fault.

Y.-G. Li, P. Leary, K. Aki, Department of Geological Sciences, University of Southern California, Los Angeles, CA 90089.
P. Malin, Department of Geological Sciences, University of California, Santa Barbara, CA 93106.

wave phases, the fundamental mode and the first higher mode (top trace, Fig. 4), are evident in the data. Both phases show the dispersive character of wave-guided energy: the lower frequency components of each phase arrive earlier than the higher frequency components. The trapped waves were excited by an event A (Fig. 3). The importance of the location for observation of fault zone trapped waves is illustrated when seismograms recorded at MM are compared with those (middle traces, Fig. 4) recorded at stations FR and ED (Fig. 3). These stations recorded clear P wave and S wave arrivals but did not record trapped mode energy (above the visual detection level) because the trapped wave energy attenuated rapidly as the distance from the fault zone increased. The separation between the fundamental mode and the first higher mode increases for event P (two bottom traces, Fig. 4), which occurred closer to MM and at a shallower depth than event A. Our modeling shows that separation increases because the velocity of the fault core at the location of shallow event P is lower than that at the location of deep event A.

The sensitivity of source and receiver location relative to the low-velocity layer of the fault zone is further illustrated in Fig. 5. During an 11-month period, station MM recorded trapped waves repeatedly excited by four events with magnitudes 0.57, 0.47, 0.32, and 0.92, respectively (traces A, B, C, D, Fig. 5), and all with the same rupture location [event B (Fig. 3)]. The rupture location was determined within ±250 m from network travel time data. Behind the S wave are overlapping fundamental and first higher modes. The trapped waves excited by these events are modeled in trace E. Two other events that occurred a few hundred meters to the southwest of those four events gave similar direct body wave arrivals but did not excite trapped modes (traces F and G, Fig. 5) because they originated outside the low-velocity fault core layer. Records H and I (two bottom traces, Fig. 5) from station ED for the event that generated trapped waves at MM (trace A) and the event that did not generate trapped waves at MM (trace F), respectively, show the closely similar P and S arrivals but do not show trapped waves. The seismograms of Fig. 5 show that the trapped mode observations are repeatable and that the source must be in the fault core layer (traces F and G versus A to D) and the receiver must be near the fault zone (trace H versus A) for detection.

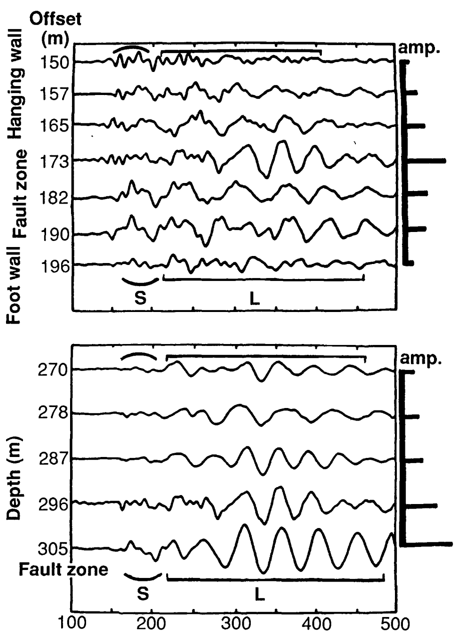

Fig. 2. (**Top**) Oroville SH-Love waves recorded at depth of 295 m for a range of source offsets from the wellhead across the fault. Traces have a common amplitude scale. Bars to right give maximum amplitude (amp) of each trace. SH wave and trapped modes are marked by S and L, respectively. (**Middle**) SH-Love waves recorded at borehole depths of 270 to 305 m for a source at the center of the fault surface trace. (**Bottom**) Computed trapped wave forms at a depth of 305 m for the fault zone model in Fig. 1.

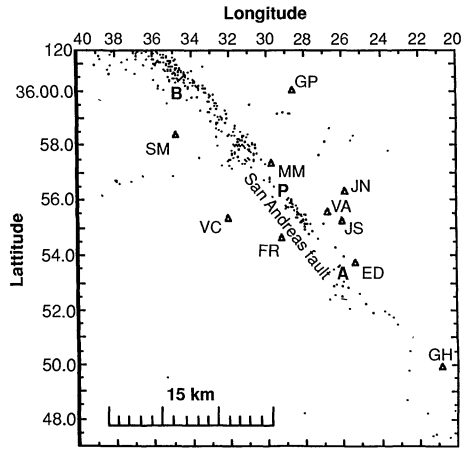

Fig. 3. Parkfield downhole digital seismic network stations (triangles) and microearthquake epicenters, 1987 to 1989 (dots). A, B, and P locate events exciting fault zone trapped waves recorded at station MM. A, magnitude 1.2, depth 10 km, epicenter 12 km southeast of MM; B, magnitude 0.57, depth 4 km, epicenter 11 km northwest of MM; P, magnitude 0.39, depth 3.9 km, epicenter 3.5 km southeast of MM. Station ED is offset 1.5 km east of the fault. FR is offset 2 km west of the fault; MM, Middle Mountain; GP, Gastro Peak; JN, Joaquin North; JS, Joaquin South; ED, Eades; P, Parkfield; GH, Gold Hill; FR, Frolich; VC, Vineyard Canyon; SM, Stockdale Mountain; and VA, Varian.

The trapped waves recorded at Parkfield have been modeled with the simplest possible physical theory (SH-Love wave), the simplest component of motion (vertical), and the simplest wave guide model (infinit, uniform, parallel, nonattenuating media) to obtain an initial estimate of the fault zone wave guide properties. However, our use of SH trapped waves for wave guide modeling is dependent on the fault geometry in layered crust parallel to the vertical fault plane but where the wave guide is vertically uniform and the source-receiver distance is long, fault-parallel SH motion will appear largely as vertical displacement at the receiver along the fault. If, on the other hand, the source-receiver distance is short and fault zone–guided energy propagates subvertically, our physical modeling will have to be suitably revised. The fault zone wave guide structure at Parkfield used in our modeling is motivated by a combination of observation and modeling experience with data from fault zone vertical seismic profiling (VSP) at Oroville.

Using the four-layer fault zone structure of Fig. 1, we computed the trapped mode wave forms for events A, B, and P and compared the best fit structural parameters for trapped waves generated by deep event A, in the locked fault sector with those of shallow event P in the locked sector and with those of event B in the creeping sector (Table 1). The most sensitive parameters are the width and velocity of the fault core layer, and there is a trade-off between them with regard to the effect on trapped mode wave forms. In order to examine the trade-off

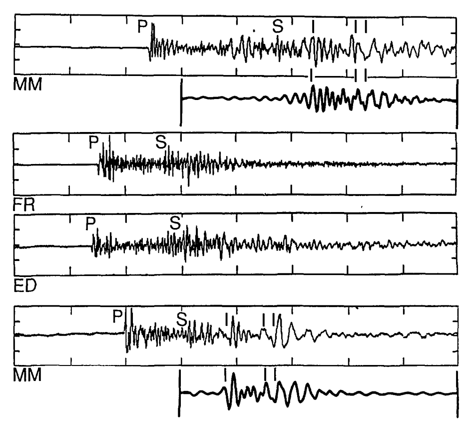

Fig. 4. (**Top**) Vertical component seismograms recorded at station MM for event A and the computed trapped wave forms for four-layer fault zone model (Table 1). P wave, S wave, fundamental and first higher modes of trapped waves are marked by P, S, II, and I. (**Middle**) Two seismograms recorded at stations FR and ED. (**Bottom**) Seismograms recorded at station MM for event P and the computed trapped wave forms. Time span is 1 s. The name of recording station is at left bottom of each panel.

carefully, we computed synthetic seismograms for 150 pairs of these two parameters in the range of 50 to 200 m of width at 10-m intervals and of 1.0 to 2.0 km/s of velocity at 0.1-km/s intervals. We obtained the best fit to observations with those values listed in Table 1, and we could not explain both fundamental and first higher modes simultaneously in the peripheral region of the parameter space studied. The modeled velocity values of the transition layer and enclosed crustal blocks are consistent with those determined from direct body wave arrival times (*3*). The decrease of the velocity contrast between the highly damaged fault core and its surrounding rocks from location A to B along the fault parallels the transition from a wholly locked fault part south of Parkfield to a fully creeping part north of Parkfield (*9*). Events P and B, which have the same focal depth, show the same style of contrast. However, the fault at the P event location in the locked sector has a thinner core layer with lower velocity than does the fault in the creeping sector, and these relations suggest that the degree of rock damage is locally higher at Parkfield during recurrent M = 6 faulting episodes (*9*).

The observation of fault zone–guided waves at Parkfield indicates that the SAF has a narrow core layer. High resolution direct wave travel time inversion of local network data (*10*) and surface sources (*11*) have demonstrated that there is a velocity contrast across the fault and there is a broad low-velocity zone associated with the fault trace. This low-velocity zone probably corresponds to a combination of the fault core layer and the transition zone shown by our data. Our modeling of the fault structure at Oroville and at Parkfield (*4*) suggests that the rupture plane proper is the core layer. Transition zones at Oroville and Parkfield are undoubtedly related to the faulting process but are more likely by-products of faulting rather than critical elements in the rupture nucleation process. For instance, at Oroville the transition zone may be a result of proximity to the free surface of the hanging wall rock, where stress trajectories diverge from the fault plane and the strain field broadens in the unconfined near surface rock. At Parkfield, in light of the observed differences in rock type between the east and west sides of the SAF (*3, 9*), we suggest that the transition zone may be caused by the lower strength of the rocks in the eastern Franciscan block whereas such a zone may be absent in the granitic rocks on the west (*1, 12*).

Fundamental to the seismic recurrence cycle, we suggest, is the low-velocity fault core layer [or fault gouge (*12*)] resolved by our trapped wave data. On a macroscopic scale, this low-velocity rupture zone should be the major structural breakdown zone controlling the seismic release of crustal stress. If laboratory models of fault-slip nucleation are correct, the core layer will be the plane on which episodes of slip-weakening occur immediately before the main rupture (*13*). Laboratory models cannot, however, reproduce the full complexity of the crust, including variations of crustal properties along the fault and with depth. The high velocity contrast between the fault gouge and surrounding rocks at A, where the background seismicity is low (*8*), implies that the fault is strong and the adjacent rock is stiff. This sector is plausibly thought to be currently building up to seismic release (*7*). At the area of B, the lower velocity contrast implies that the surrounding rock is weaker and thus that the fault is more easily broken on shorter distance and time scales. Small microearthquakes as well as surface creep occur regularly on this sector of the fault.

On a microscopic scale, we presume that the fault gouge zone contains the highly damaged rock produced by active sliding and is the nucleation surface of the anticipated recurrent magnitude 6 main event (*7*). The constructive interference conditions of seismic trapped waves offer information on the physical properties of the low-velocity structure of the fault zone. Equally important is the condition that a seismogram containing trapped modes must originate with a source event in the low-velocity fault gouge. From a systematic inspection of the Parkfield downhole seismic network catalog, a subcatalog of events can be assembled consisting of those events originating in the narrow confines of the fault core layer. Such a catalog of events serves two functions. First, as the events lie on essentially a plane, the location of seismic event hypocenters provides a strong spatial constraint on permissible event locations. This constraint can lead to a refined velocity profile for the entire catalog of earthquake events. Second, events originating in the low-velocity fault core layer can be investigated for source mechanism parameters such as elastic rigidity, rupture velocity, inhomogeneity scale length, breakdown zone dimension, S to P spectral ratio, corner frequency and the maximum frequency that are specific to the fault plane itself (*14*).

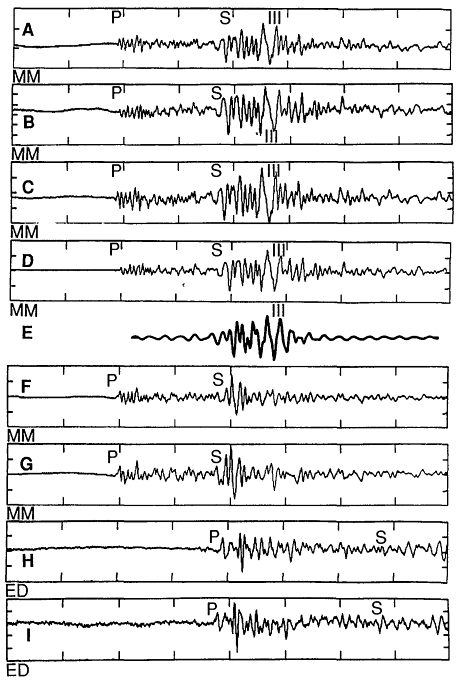

Fig. 5. (**A**) Vertical seismogram recorded at station MM for event B. P wave, S wave, and trapped modes are marked by P, S, and III. The fundamental and higher modes overlap. (**B, C, D**) MM seismograms for events originating near B in the fault core layer but at different times over an 11-month period. (**E**) Computed wave form for B (Table 1). (**F** and **G**) MM seismograms for two events near B hypocenter but outside the fault core layer; no trapped waves were excited. (**H** and **I**) Station ED seismograms for event B and event G. While the P and S waves are closely similar, B in the fault zone generated trapped waves whereas event G outside the fault zone generated no trapped waves. Time span is 1 s.

Table 1. Fault zone wave-guide model parameters as function of source position; ν, velocity.

Parameter	Event		
	A	P	B
Location from MM (km)	12 SE	3.5 SE	11 NW
Depth (km)	10	4	4
Core layer width (m)	100	110	160
Core layer ν (km/s)	1.4	1.1	1.8
Transition layer width (m)	350	350	400
Transition layer ν (km/s)	2.55	1.80	2.40
Western crustal block ν (km/s)	2.95	2.20	2.75
Eastern crustal block ν (km/s)	2.80	2.10	2.60

REFERENCES AND NOTES

1. W. D. Mooney and A. Ginzburg, *Pure Appl. Geophys.* **124**, 141 (1986).
2. P. C. Leary, Y. G. Li, K. Aki, *Eos* **66**, 976 (1985); *Geophys. J. R. Astron. Soc.* **91**, 461 (1987); Y. G. Li, P. C. Leary, K. Aki, *ibid.*, p. 485; Y. G. Li, thesis, University of Southern California (1988).
3. J. H. Lees and P. E. Malin, *J. Geophys. Res.*, in press; A. Michilini, W. Foxall, T. V. McEvilly, *Seismol. Res. Lett.* **60**, 31 (1989); J. P. Eaton, M. E. O'Neill, J. N. Murdock, *Bull. Seismol. Soc. Am.* **60**, 1151 (1970).
4. Y. G. Li and P. C. Leary, *Bull. Seismol. Soc. Am.*, in press.
5. K. Aki and P. G. Richards, *Quantitative Seismology* (Freeman, San Francisco, 1980).
6. W. H. Bakun and A. G. Lindh, *Science* **229**, 619 (1985).

7. W. H. Bakun and T. V. McEvilly, *ibid.* **205**, 1375 (1979); *J. Geophys. Res.* **89**, 3051 (1984).
8. P. E. Malin, S. N. Blakeslee, M. G. Alvarez, A. J. Martin, *Science* **244**, 557 (1989), T. V. McEvily *et al.*, *U.S. Geol. Surv. Open-File Rep. 89-453* (1989), p. 333.
9. K. Aki, *J. Geophys. Res.* **84**, 6140 (1979); W. D. Mooney and J. H. Luetgert, *Bull. Seismol. Soc. Am.* 72, 901 (1982); A. P. Papageorgiou and K. Aki, *ibid.* 73, 953 (1983).
10. K. Aki and W. H. K. Lee, *J. Geophys. Res.* **81**, 4381 (1976); C. H. Thurber, *ibid.* **88**, 8226 (1976).
11. R. Feng and T. V. McEvilly, *Bull. Seismol. Soc. Am.* **73**, 1701 (1983); J. N. Louie, R. W. Clayton, R. J. LeBras, *Geophysics* **53**, 176 (1988).
12. C. Y. Wang, *J. Geophys. Res.* **89**, 5858 (1984).
13. J. H. Dietrich, *ibid.* **84**, 2161 (1979); *ibid.*, p. 2169; W. D. Stuart, R. Archuleta, A. G. Lindh, *ibid.* **92**, 592 (1985); T. Cao and K. Aki, *Pure Appl. Geophys.* **122**, 10 (1984/85).
14. K. Aki, *J. Geophys. Res.* **92**, 1349 (1987); P. Okubo and K. Aki, *ibid.*, p. 345.
15. This investigation was supported in part by DOE contract DE-FG03-87ER13807 and by NSF grants EAR-8213145 and EAR-8519938.

19 March 1990; accepted 8 June 1990

Precessional Forcing of Nutricline Dynamics in the Equatorial Atlantic

B. Molfino and A. McIntyre

Climate control of nutricline depth in the equatorial Atlantic can be monitored by variations in the abundance of the phytoplankton species *Florisphaera profunda*. A conceptual model, based on in situ evidence, associates high abundances of *F. profunda* with a deep nutricline and low abundances with a shallow nutricline. A 200,000-year record of *F. profunda* relative abundances, obtained from a deep-sea core sited beneath the region of maximum equatorial divergence at 10°W, has 52 percent of its variance centered on the 23,000-year precessional band. Cross-spectral analysis between the signals of *F. profunda* and sea-surface temperature, independently derived from zooplankton species, shows their 23,000-year cycles to be coherent and nearly in phase. Abundance minima of *F. profunda* coincide with times of December perihelion, whereas abundance maxima coincide with June perihelion. These relations indicate that nutricline dynamics in the divergence region of the equatorial Atlantic are controlled by variations in the tropical easterlies, forced by the precessional component of orbital insolation, on time scales greater than 10,000 years.

The Turbulent Boundary Layer (TBL) is the upper layer of the ocean where exchange of heat and mass occurs between the oceanic and atmospheric reservoirs. The physical oceanography of the TBL is a major factor in atmosphere-ocean dynamics on all time scales. On time scales encompassed by the instrumental record, knowledge of the observed and modeled annual and interannual dynamics of the TBL is progressing rapidly (*1*). On paleoceanographic time scales, knowledge of the structure of the TBL is lacking. Paleoindicators that vertically partition the TBL to measure the character of the layers (above and below the thermocline) are needed. In this report, we present a conceptual model of the coccolithophorid (chrysophycean) species *F. profunda*. Our model is based on in situ observation, and it allows us to predict *F. profunda* variations as a function of nutricline dynamics. We applied this model to the oceanic sediments of the equatorial Atlantic in two ways: (i) spatially, using a meridional transect of modern sediment samples that compares *F. profunda*'s response to known variations of nutricline depth; and (ii) temporally, using a 200,000-year record of *F. profunda* response from one core in this transect. This species shows that nutricline dynamics in the equatorial Atlantic respond to the precessional component of insolation forcing.

B. Molfino, Lamont-Doherty Geological Observatory of Columbia University, Palisades, NY 10964, and Department of Statistics, Columbia University, New York, NY 10027.
A. McIntyre, Lamont-Doherty Geological Observatory of Columbia University, Palisades, NY 10964, and Department of Geology, Queens College of the City University of New York, Flushing, NY 11357.

Okada established the gross biogeography and ecology of *F. profunda*. This marine alga is restricted to the lower euphotic zone at temperatures >10°C (*2*), as documented for tropical and subtropical TBLs of the Pacific and the Atlantic oceans (*2–4*). All other coccolithophorids that are preserved in the fossil record are restricted to the upper euphotic zone. *Florisphaera profunda* produces subrectangular calcite plates (mean of 2.5 μm) that are easily recognized in the electron microscope and are well preserved in oceanic sediments (*2*).

We suggest that *F. profunda* can be used to monitor variations in the depth of the nutricline. Our conceptual model uses a partitioned euphotic zone in which the controlling mechanism is variation in nutrient concentration of the upper euphotic zone (Fig. 1). The random variable is the depth of the nutricline; the response variables are the number of *F. profunda* and the number of other coccolithophorids. A deep nutricline means the upper euphotic zone is nutrient-depleted and hence *F. profunda*'s production is enhanced relative to other coccolithophorids; a shallow nutricline has the opposite effect. We identified 500 individuals per sample and computed the percentage of *F. profunda* in the total sample as our measure of variation. The sample counts are binomially distributed; their statistical error (95% confidence limits based on binomial proportions, $n = 500$) is approximately ±4% for values between 30 and 70% (*5*).

In the equatorial Atlantic, alternating ribbons of high and low primary productivity are aligned along parallels of latitude (*6*). These ribbons are produced by the seasonally varying surface currents of the South

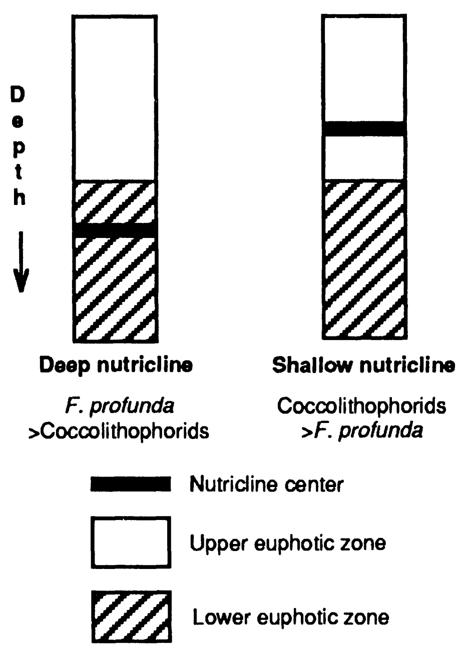

Fig. 1. The conceptual model of *F. profunda* response to variation in nutricline depth is illustrated with two end member scenarios. *Florisphaera profunda* is restricted to the lower part of the euphotic zone, while all other coccolithophorid species inhabit the upper euphotic zone. A deep nutricline enhances the production of *F. profunda* over all other coccolithophorid species (left). A shallow nutricline enhances the production of other coccolithophorid species relative to *F. profunda* (right).